Science Signaling
AAAS

www.sciencesignaling.org/cgi/content/full/8/378/ra50/DC1

Supplementary Materials for

A large-scale screen reveals genes that mediate electrotaxis in *Dictyostelium discoideum*

Runchi Gao, Siwei Zhao, Xupin Jiang, Yaohui Sun, Sanjun Zhao, Jing Gao, Jane Borleis, Stacey Willard, Ming Tang, Huaqing Cai, Yoichiro Kamimura, Yuesheng Huang, Jianxin Jiang, Zunxi Huang, Alex Mogilner, Tingrui Pan, Peter N. Devreotes, Min Zhao*

*Corresponding author. E-mail: minzhao@ucdavis.edu

Published 26 May 2015, *Sci. Signal.* **8**, ra50 (2015)
DOI: 10.1126/scisignal.aab0562

This PDF file includes:

Other Supplementary Material for this manuscript includes the following:
(available at www.sciencesignaling.org/cgi/content/full/8/378/ra50/DC1)

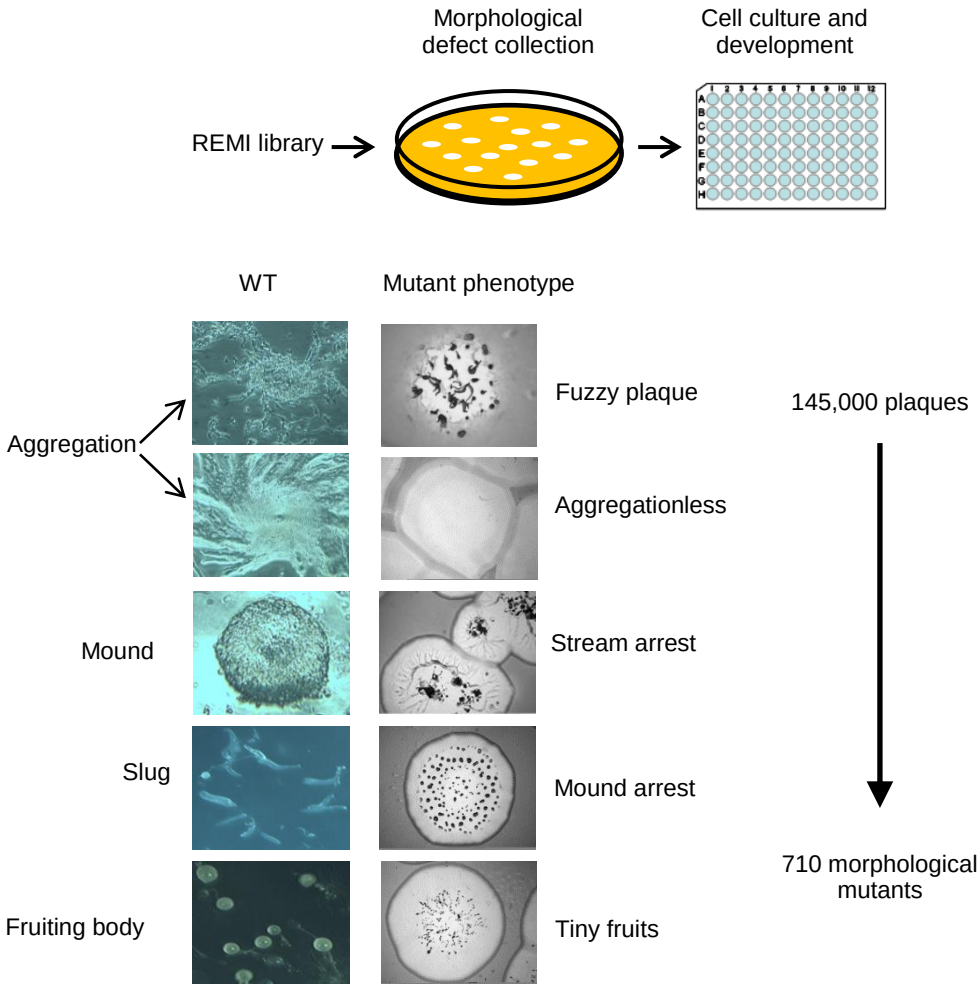

Fig. S1. The collection of mutant strains with morphological defects used in our screen.

A set of mutants with morphological defects were selected from a REMI library. Individual cells plated on bacterial lawns grew within a few days to form ~1cm plaques. The genetically identical cells within the plaque aggregated and differentiated to form multicellular structures. If the original cells bore a genetic defect that acted early in the developmental program, the plaque formed, but the cells remained as a monolayer. When cells developed further to form mounds or slugs, the size of mounds and slugs and the number of culminating heads provided a second set of criteria for defining the morphological phenotype. The size and number of fruiting bodies was the third criterion. About 710 morphological defect mutants were collected from 145,000 mutants. These were: aggregationless (202 mutants), tiny fruits (167 mutants), culmination defect (135 mutants), mound arrest (87 mutants), stalk/spore defect (79 mutants), stream arrest (32 mutants), and fuzzy plaque (8 mutants).

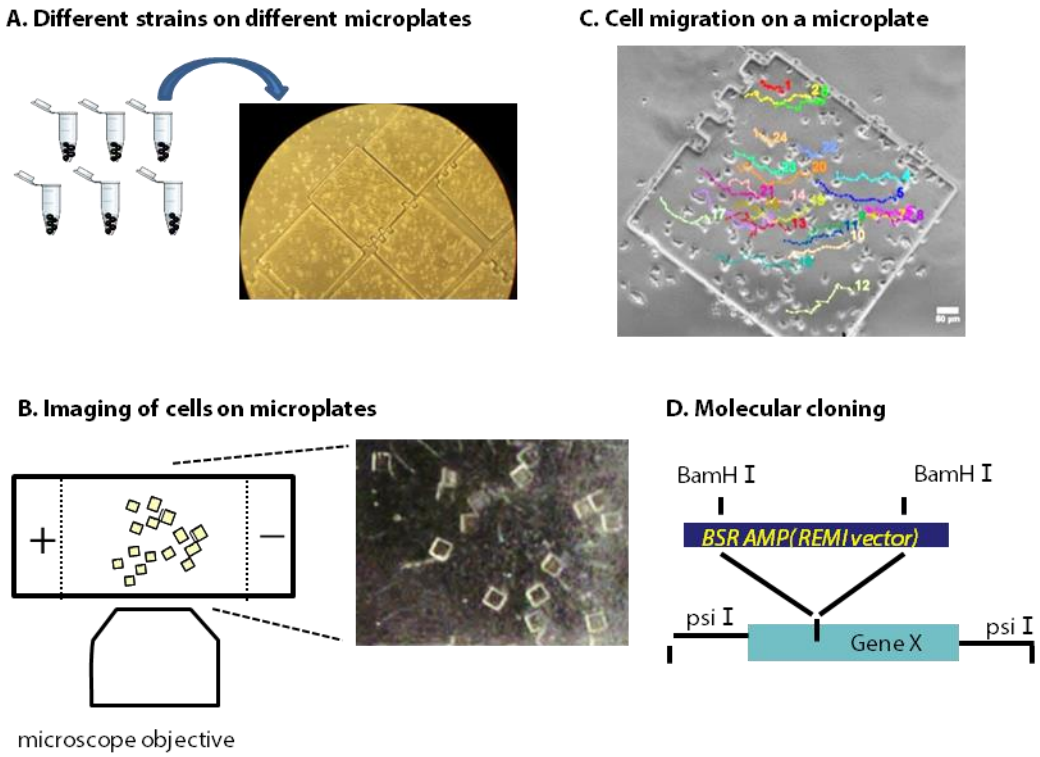

Fig. S2. High-throughput screening strategy to determine electrotaxis phenotypes.

A. Seeding cells from individual strains on bar-coded microplates of polyethylene glycol (PEG) hydrogel.

B. Multiple bar-coded microplates were loaded into an electrotaxis chamber, which was placed on a microscope stage for multi-field time-lapse digital imaging, thereby allowing simultaneous screening for electrotaxis phenotype of many strains at the same time. The photograph on the right shows a microscopic field with multiple microplates.

C. A typical micrograph of a bar-coded microplate with cells, and migration trajectories (colored lines) of cells tracked with ImageJ superimposed on the microplate.

D. Molecular cloning of the site of insertion and the flanking DNA.

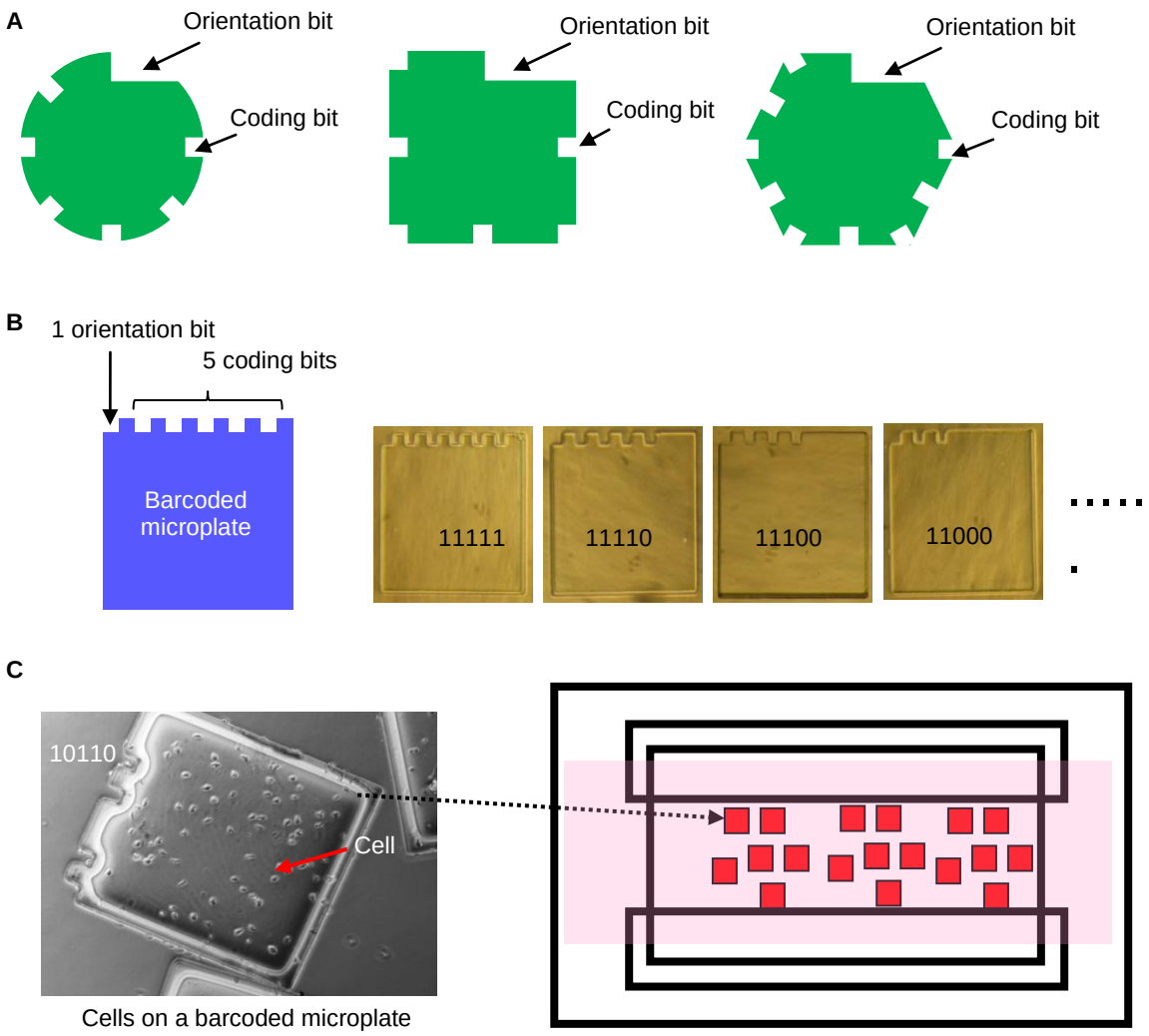

Fig. S3. Design and fabrication of the barcoded microplates.

A. A large number of coded microplates could be made in circular, hexagonal, or square shapes. Each microplate included one orientation bit indicating the start position and reading direction of the barcode. Coding bits identified individual barcoded microplates, which contained specific cell strains. The size of the plates used in this study were in the 100mmx100 mm to 500mmx500mm range.

B. A square microplate design was employed for large migration area and easy barcode placement. A five-digit binary barcode was designed to encode hundreds of strains of mutated *Dictyostelium* cells.

C. A microplate loaded with cells (left). Many plates with different strains could be loaded into an electrotaxis chamber for high throughput electrotaxis experiments.

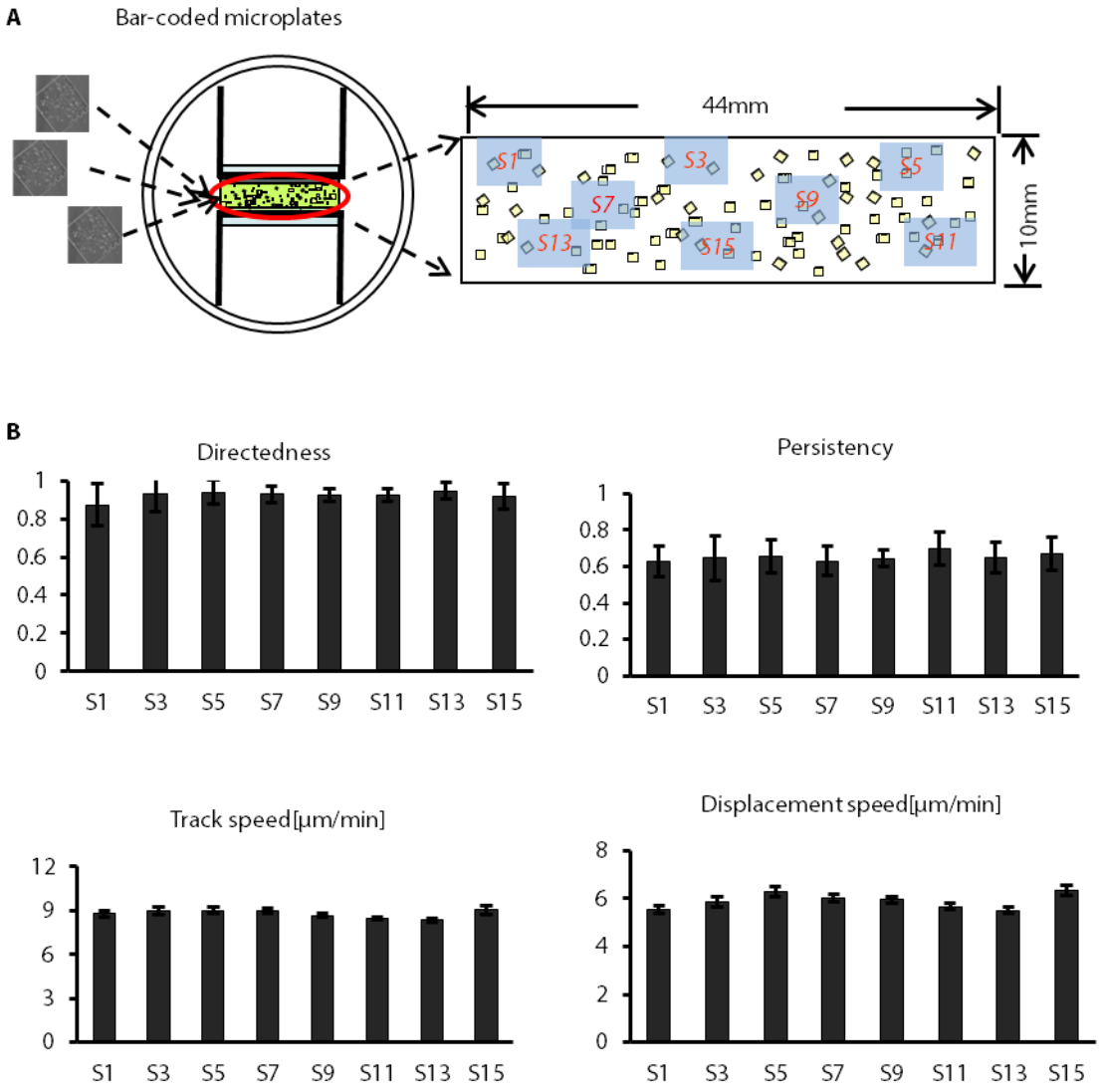

Fig. S4. Cells on barcoded microplates at different positions in an electrotaxis chamber showed consistent electrotaxis responses.

A. A schematic diagram shows selected positions in an electrotaxis chamber where cell migration was recorded and analyzed.

B. Quantitative analyses of cell migration at eight different positions in an electrotaxis chamber showed consistent electrotaxis responses. Directedness, persistence, track speed and displacement speed were similar at all positions. EF= 12V/cm. Data (mean ±SEM) for each position were quantified from 50 cells per condition in three independent experiments.

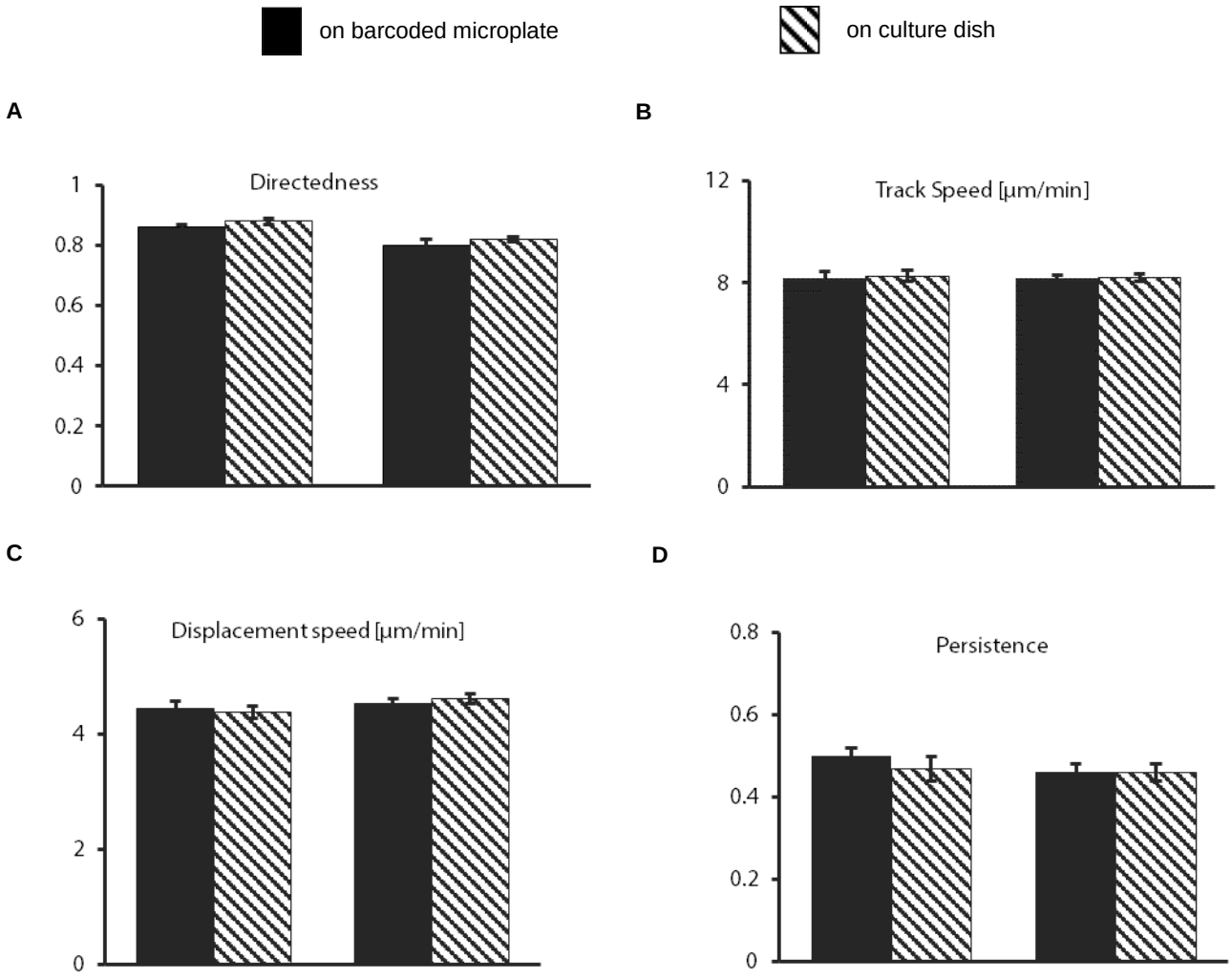

Fig. S5. *Dictyostelium* cells displayed consistent migration phenotypes on both barcoded microplates and on tissue culture dishes.

AX2 and AX3 cells displayed the same electrotaxis response on barcoded microplate material and culture dish plates. n=40~50 cells per condition from at least three independent experiment.

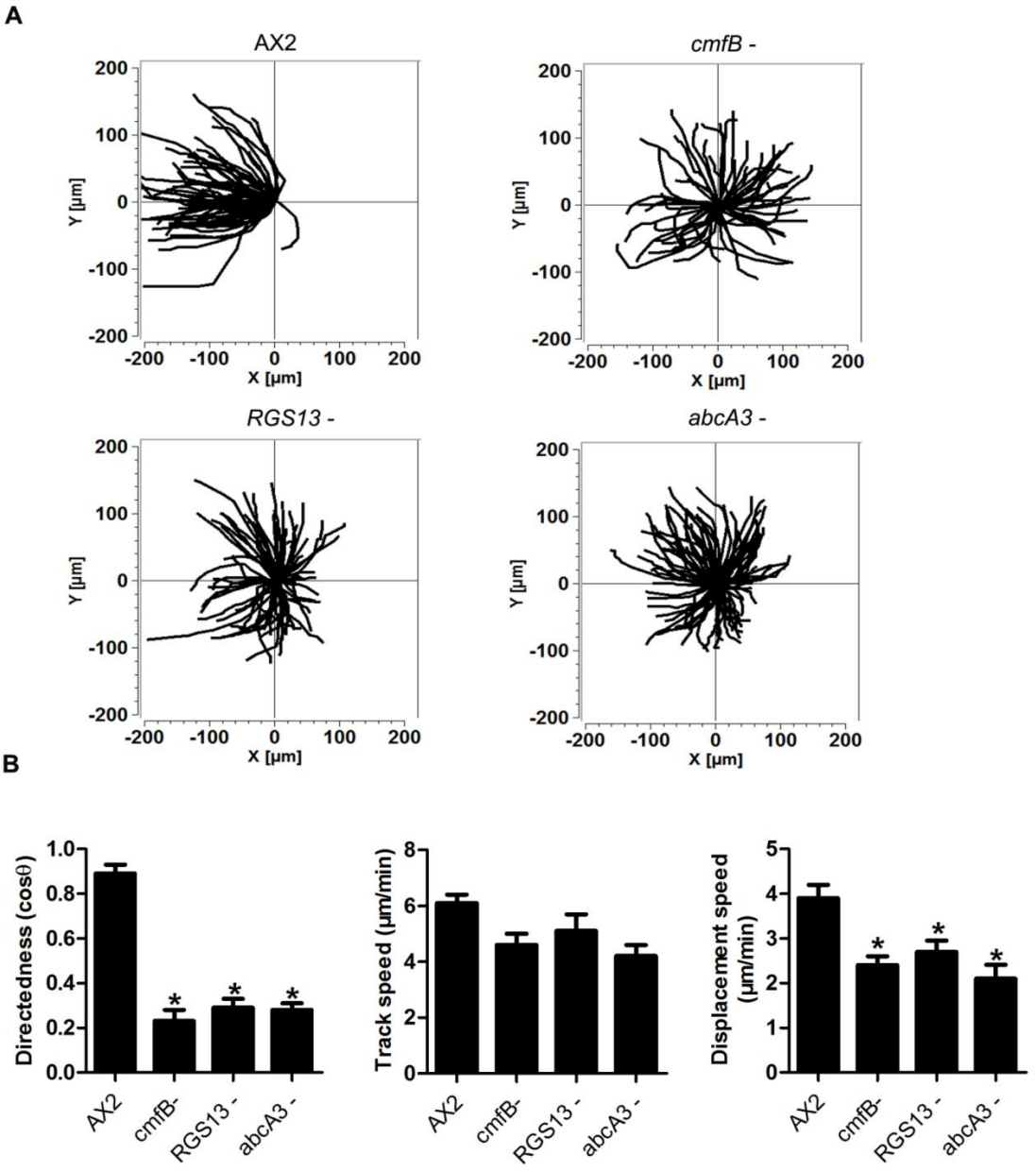

Fig. S6. Recapitulation of the defective electroxis phenotype in the mutant strains by knockout cells.

A. Electrotaxis of knock-out strains (*cmfB-, RGS13-* and *abcA3-*). Cell migration trajectories are presented with the start point of each cell set as the origin. WT cell (AX2) migrated directionally towards the cathode (to the left). Electrotaxis was significantly impaired in *cmfB-, RGS13-* or *abcA3-* cells.

B. *cmfB-, RGS13-* or *abcA3-* cells showed significantly decreased directedness values, without significant effects on the trajectory speed.

Data are mean±s.e.m. from at least 50 cells per genotype from three independent experiments. **P < 0.01, Student's t-test, compared with AX2 WT cells.

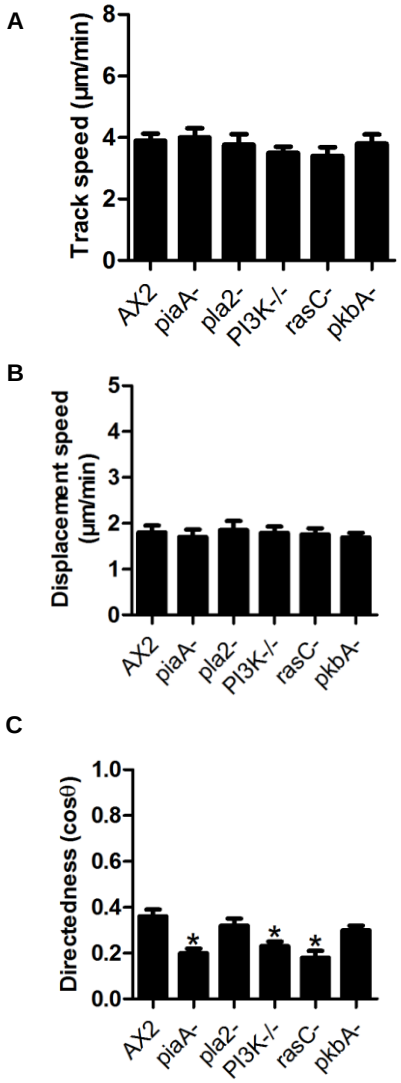

Fig. S7. Electrotaxis of vegetative cells.

A, B. Vegetative cells of different knockout strains had the similar migration speeds in an electric field.

C. Different mutated cells (*piaA-,PI3K-/- and rasC-*) showed significantly decreased electrotaxis.

Data are mean± s.e.m. from at least 50 cells per genotype from three independent experiments. *: $p<0.05$ when compared with wild-type (Ax2) cells in an electric field of the same strength.

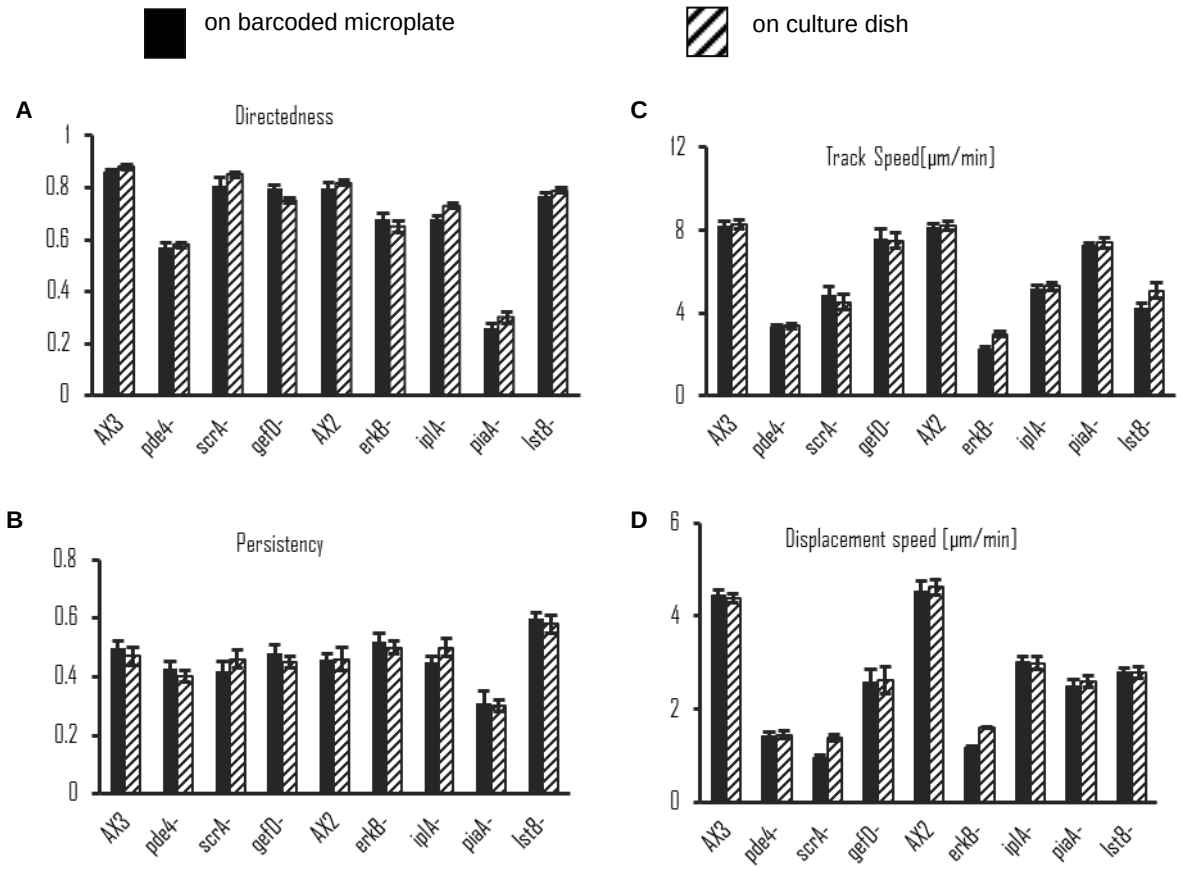

Fig. S8. Mutated strains of *Dictyostelium* cells displayed consistent migration phenotypes on barcoded microplates and tissue culture dishes.

AX2, AX3 and selective mutants strains displayed the same electrotactic response on barcoded microplates and culture dishes. n=40~50 cells per genotype from at least three independent experiment.

Table S1. Defective strains identified from the screen.

Strain	directedness	persistency	track speed (μm/min)	displacement speed (μm/min)
WT	(-)0.90±0.03	0.57±0.02	6.08±0.21	3.48±0.16
SN-129	(-)0.08±0.02	0.31±0.01	4.63±0.32	1.44±0.12
SN-576	(-)0.16±0.02	0.34±0.03	2.50±0.14	1.24±0.18
SN-183	(-)0.17±0.02	0.32±0.02	7.63±0.40	3.24±0.31
SN-494	(-)0.19±0.11	0.41±0.03	7.68±0.41	3.28±0.34
SN-517	(-)0.20±0.10	0.26±0.12	5.17±0.29	1.42±0.13
SN-028	(-)0.21±0.09	0.26±0.02	6.00±0.27	1.57±0.14
SN-447	(-)0.21±0.10	0.30±0.02	3.48±0.15	1.05±0.11
SN-613	(-)0.22±0.12	0.33±0.03	6.54±0.35	2.25±0.30
SN-677	(-)0.22±0.10	0.31±0.02	5.27±0.23	1.65±0.15
SN-123	(-)0.22±0.10	0.30±0.02	2.66±0.13	0.82±0.10
SN-P27	(-)0.23±0.09	0.23±0.03	4.73±0.25	1.28±0.13
SN-139	(-)0.24±0.11	0.28±0.04	3.62±0.21	1.08±0.13
SN-150	(-)0.24±0.10	0.27±0.02	4.70±0.19	1.28±0.10
SN-333	(-)0.25±0.02	0.32±0.01	4.79±0.33	1.51±0.22
SN-598	(-)0.20±0.10	0.30±0.02	6.59±0.34	2.21±0.29
SN-584	(-)0.20±0.11	0.35±0.02	7.29±0.40	2.61±0.25
SN-106a	(-)0.21±0.11	0.36±0.03	5.88±0.30	2.16±0.23
SN-040	(-)0.21±0.11	0.33±0.02	5.49±0.24	1.88±0.19
SN-470	(-)0.23±0.12	0.29±0.02	4.94±0.34	1.49±0.19
SN-165	(-)0.24±0.07	0.31±0.02	3.82±0.19	1.20±0.14
SN-661	(-)0.25±0.13	0.31±0.03	8.66±0.48	2.84±0.35
SN-242	(-)0.26±0.11	0.37±0.02	4.89±0.29	1.74±0.15
SN-252	(-)0.27±0.10	0.26±0.02	8.93±0.43	2.40±0.33
SN-223	(-)0.28±0.12	0.35±0.03	10.30±0.81	4.03±0.53
SN-290	(-)0.28±0.10	0.41±0.02	7.21±0.44	2.94±0.26
SN-432	(-)0.29±0.10	0.34±0.03	7.76±0.42	2.88±0.38
SN-403	(-)0.29±0.11	0.39±0.03	7.51±0.49	3.15±0.43

SN-170	(-)0.29±0.12	0.29±0.03	7.01±0.34	3.05±0.24

Table S2. Hyperresponsive strains identified.

Strain	directedness	persistency	track speed (μm/min)	displacement speed (μm/min)
WT	(-)0.90±0.03	0.57±0.02	6.08±0.21	3.48±0.16
SN-657	(-)0.91±0.02	0.52±0.03	7.05±0.42	3.79±0.37
SN-269	(-)0.91±0.03	0.59±0.03	7.09±0.57	4.24±0.38
SN-703	(-)0.91±0.02	0.64±0.02	7.76±0.26	4.99±0.25
SN-201	(-)0.92±0.01	0.54±0.01	5.94±0.33	3.33±0.23
SN-016	(-)0.92±0.02	0.48±0.02	4.02±0.17	2.01±0.15
SN-141	(-)0.92±0.02	0.54±0.02	4.41±0.18	2.42±0.15
SN-272	(-)0.93±0.01	0.51±0.01	4.77±0.23	2.53±0.13
SN-052	(-)0.94±0.01	0.59±0.01	3.57±0.22	2.23±0.12
SN-658	(-)0.95±0.01	0.58±0.01	4.57±0.31	2.67±0.11
SN-653	(-)0.95±0.05	0.47±0.03	5.68±0.22	2.77±0.21
SN-301	(-)0.97±0.01	0.67±0.01	7.73±0.43	5.28±0.31

Table S3. Knockouts confirmed the genes that underlie the 12 defective strains.

Abbreviation	Strains names	Origins	Source
gefA-	*gefA* knockout	AX3	DictyBase
rasC-	*rasC* knockout	AX2	Devreotes Lab
piaA-	*piaA* knockout	AX3	Devreotes Lab
rip3-	*rip3* knockout	AX3	Devreotes Lab
lst8-	*lst8* knockout	AX2	Devreotes Lab
pkbA-	*pkbA* knockout	AX2	Devreotes Lab
pkbR1-	*pkbR1* knockout	AX2	Devreotes Lab
pla2-	*pla2* knockout	AX2	Devreotes Lab
piaA-/pla2-	*piaA* and *pla2* knockout	AX2	Devreotes Lab
cmfB-	*cmfB* knockout	AX2	Devreotes Lab
rgs13-	*RGS13* knockout	AX2	Devreotes Lab
abcA3-	*abcA3* knockout	AX2	Devreotes Lab
pi3k-/-	*Pi3k1* and *pi3k2* double knockout	AX2	Devreotes Lab

Movie S1. Wild-type AX2 cell not in an electric field. The video was recorded every one minute for 30 minutes.

Movie S2. Wild-type AX2 cell in an electric field of 12 V/cm. The video was recorded every one minute for 30 minutes. The negative pole is on the left and the positive pole is on the right.

Movie S3. *PiaA*$^{-}$ cell in an electric field of 12 V/cm. The video was recorded every one minute for 30 minutes. The negative pole is on the left and the positive pole is on the right.

Movie S4. Reexpression of piaA in *piaA*$^{-}$ cells restored electrotaxis. The electrotaxis assays were conducted in an electric field of 12V/cm. The video was recorded every one minute for 30 minutes. The negative pole is on the left and the positive pole is on the right.